An Experimental Parametric Study on the Whirl-Flutter Stability of Tiltrotors

Robert P. Thornburgh
DEVCOM ARL
Hampton, VA, USA

Andrew R. Kreshock
DEVCOM ARL
Hampton, VA, USA

Hao Kang
DEVCOM ARL
Aberdeen Proving Ground, MD, USA

Thomas G. Ivanco
NASA
Hampton, VA, USA

Martin K. Sekula
NASA
Hampton, VA, USA

Garrett R. McHugh
NASA
Hampton, VA, USA

ABSTRACT

This paper presents an overview of the results from the second wind-tunnel test of the TiltRotor Aeroelastic Stability Testbed (TRAST). The objective of this test was to obtain experimental data for understanding the effects of tiltrotor parameters on whirl flutter and analysis-validation data for the prediction of whirl flutter across a range of system configurations. Frequency and damping were measured at multiple rotor speeds for pitch-flap-coupling angles ranging from -0° to -30°. In addition, measurements were made for changes in blade stiffness, air density and wing-pylon connection stiffness. The paper also presents the results from supporting measurements that may aid analysis validation, such as wing-only damping, rotor frequencies and non-spinning modal frequencies.

INTRODUCTION

The TiltRotor Aeroelastic Stability Testbed (TRAST) is an aeroelastic tiltrotor testbed that was developed by the U.S. Army and NASA to investigate whirl-flutter stability of tiltrotor aircraft (Ref. 1). It is one of a number of wind-tunnel testbeds that have been developed in recent years to study this challenging aeroelastic phenomenon (Refs. 2-4). The TRAST is a semi-span model and consists of a starboard wing, a rigid fuselage/fairing, and a pylon that supports an 8-ft-diameter rotor (Figure 1). Although the TRAST is a generic tiltrotor model representative of a typical tiltrotor aircraft configuration, it was designed for parametric studies of key control-system values and structural stiffnesses.

An initial wind-tunnel test of the TRAST was performed in the NASA Langley Transonic Dynamic Tunnel (TDT) in late 2021 to characterize the stability boundary of the baseline system and identify any problems with the newly built model. During this test, system damping was found to be much larger than expected (Ref. 5). Following this test, a series of model changes were implemented to reduce friction in the gimbal and conversion bearing, resulting in more realistic structural damping for the model. In addition, a new test procedure for stability data was developed that would produce a more accurate and consistent set of stability measurements in the wind tunnel.

A follow-on wind-tunnel test was conducted by U.S. Army DEVCOM and NASA from October to December 2023 in the TDT, with the objective of obtaining a robust set of experimental data for test-analysis correlation of rotorcraft comprehensive modeling tools, such as CAMRAD II and RCAS. To accomplish this goal, the wind-tunnel test included a large parametric study of various pitch-flap-coupling angles (δ_3), different pylon mounting stiffnesses, and structurally different blade sets. This paper presents the stability measurements from this second wind-tunnel test and the results of the parametric studies that were performed. In

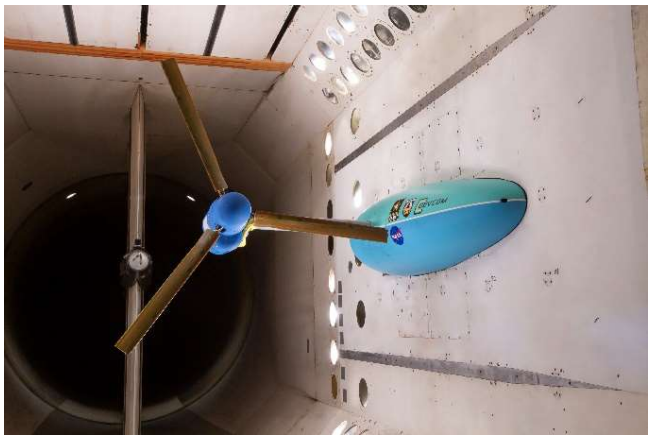

Figure 1. TRAST in the Langley Transonic Dynamics Tunnel.

Presented at the Vertical Flight Society's 81st Annual Forum & Technology Display, Virginia Beach, VA, USA, May 20-22, 2025.

addition, it will describe the testing process, discuss observations made during the test, and present other experimental measurements that support the validation of comprehensive models of the TRAST.

TESTBED FEATURES

The key feature of the TRAST (Ref. 5) that makes it particularly suitable for obtaining data for analysis validation is its relative reconfigurability when compared to other tiltrotor testbeds. While the stiffness of the wing cannot be easily altered, the model has two springs that allow the stiffness of the connection between the pylon and the wing to be modified during the wind-tunnel test. There is a segmented diaphragm spring that connects the static side of the conversion bearing to the wing. By replacing the spring segments the roll and yaw stiffness of the pylon can be changed. The baseline diaphragm spring has a rotational stiffness of 20,000 in-lb/rad in both the roll and yaw directions, and a half-yaw-stiffness spring can be used that has a stiffness of 10,000 in-lb/rad in the yaw direction while maintaining a 20,000 in-lb/rad stiffness in the roll direction.

In addition to the diaphragm spring, a replaceable pitch spring is used to join the pylon to the wing. Unlike a flight vehicle in which the pylon conversion angle is controlled by a displacement actuator, the TRAST pylon uses a simple linear spring to simulate the stiffness of the flight actuator. A range of pitch springs with stiffnesses between 3000 and 8000 lbf/in have been manufactured, and they can be swapped during testing for parametric studies of this important structural stiffness. During the present test, pitch springs with stiffness values of 2862, 4292 and 4852 lbf/in were tested. These are colloquially referred to herein as the 3k, 4k and 5k pitch springs, respectively.

The TRAST also was tested with two separate rotor blade sets. These blade sets were designed with identical planform and twist distributions but different structural stiffnesses. The primary set was manufactured using a fiberglass construction, while the second set was made using carbon fiber, making it significantly stiffer. A discussion of the effect of the blade stiffness on the TRAST is presented in Ref. 6.

In addition to changeable structural stiffnesses, the TRAST was designed with an adjustable pitch-flap-coupling angle in the rotor control system. By adjusting the length of the pitch horns and indexing the connection point to the swashplate, the pitch-flap coupling angle can be altered in 5-deg increments from -0° to -30° while still maintaining the verticality of the pitch links. Positive δ_3 is defined such that when the blade flaps up, the blade pitches downward. The use of negative δ_3 in tiltrotors is to avoid excessive flapping and rotor flap-lag instability.

TEST APPROACH AND STABILITY QUANTIFICATION

The wind-tunnel test was conducted in the TDT with the TRAST mounted to the side wall and operating in airplane mode. All testing was conducted in air (rather than R-134a gas) at a nominal tunnel pressure of 1900 psf, except for one configuration where measurements were also obtained at both a higher and a lower tunnel pressure to quantify the effect of air density. This nominal tunnel pressure corresponded to a test medium density of approximately 0.00209 slug/ft^3 throughout the test. Stability measurements were performed with the rotor windmilling, with the driveshaft disconnected from the motor in order to minimize rotor torque. Throughout the test campaign two rotor speeds were employed, a nominal rotor speed (NR) of 909 RPM and a reduced rotor speed of 727 RPM (0.8 NR). For a few cases, stability measurements were also obtained at an intermediate rotor speed of 818 RPM (0.9 NR).

The primary modes that were measured during testing consisted of the wing-vertical mode, which is the low-frequency vertical bending mode of the wing and pylon that typically goes unstable at the lowest airspeed, and the wing-inplane mode, which exhibits chordwise wing motion and can result in instability at high airspeeds. It should be noted that because of the mass offset of the pylon and the pitch-spring flexibility, these modes include significant amounts of pylon pitch motion as well. The pylon-pitch/wing-torsion mode and the pylon yaw mode were tracked during testing, but detailed measurement sweeps were not made, based on their observed behavior during the first wind-tunnel test. The pylon-pitch/wing-torsion mode, typically around 9.5 Hz, always exhibited damping values in excess of 5 percent. The yaw mode, around 18 Hz, exhibited a damping around 4 percent that was relatively insensitive to tunnel speed.

The parametric studies presented in this paper required hardware changes to alter the parameter being investigated and were each treated as a separate configuration. In total, 12 separate configurations were tested, and these are summarized in Table 1. Broadly speaking, the test matrix consisted of a detailed sweep across six different values of pitch-flap coupling using the fiberglass rotor blades, a coarse sweep with three values of pitch-flap coupling using the carbon-fiber rotor blades, a sweep with three pitch-spring stiffnesses, a sweep with three tunnel pressures, and a comparison between the two diaphragm-spring yaw stiffnesses.

The technique used to obtain stability measurements during this wind-tunnel test was similar to the technique detailed in Ref. 1. Once the testbed was at a steady flight condition and rotor speed, the testbed was excited by oscillating the swashplate at the frequency of the mode being measured. The aerodynamic forces induced by this oscillation would create a forced response of this mode that steadily increased until it reached a target amplitude, at which time the

Table 1. TRAST parametric study test matrix showing the pitch-spring stiffness tested for each combination of rotor speed, blade type and pitch-flap coupling.

Pitch-flap coupling, δ_3	Fiberglass Blade			Carbon-Fiber Blade	
	727 RPM	818 RPM	909 RPM	727 RPM	909 RPM
-30°	4k	4k	4k	4k	4k (1700psf, 1900psf, & 2100psf)
-25°	4k	4k	4k		
-20°	3k, 4k, 5k, 5k*	5k*	3k, 4k, 5k, 5k*		
-15°	4k	4k	4k	4k	4k
-10°	4k		4k		
-0°	4k		4k	4k	4k

3k: 2862-lb/in pitch spring, 4k: 4292-lb/in, 5k: 4850-lb/in, 5k*: 4850-lb/in pitch spring with half-yaw diaphragm spring

excitation was ended, and the free-decay response of the testbed was measured. Typically, the vertical bending moment at the wing root was used for wing-vertical-mode estimates and the chordwise bending moment at the wing root was used for wing-inplane-mode estimates. A minimum of five free-decay measurements were performed for each mode of interest at each test condition, although more were often measured at high speed where tunnel turbulence became significant, affecting data repeatability.

TURBULENCE EFFECT ON DATA ACCURACY

The process of using the free-decay measurements to estimate the system damping is complicated by the wind-tunnel turbulence that induces a quasi-random forced response on the measured system response. Traditional methods for damping estimation from free-decay signals, such as moving-block and Prony techniques, do not account for the presence of a random forced response, resulting in a large scatter in their damping estimates. At higher tunnel speeds, the steady-state vibration levels created by the turbulence begin to approach the target amplitudes of the swashplate oscillations. This turbulence-induced vibration not only adds a large random response to the free decay, but it also results in fewer cycles of model response before the signal level decays to below the steady-state noise floor. Thus, even averaging the five to ten points per test condition can be insufficient for accurately identifying the system damping at high tunnel speeds. This can be seen in the moving-block damping estimates (green triangles) presented in Figure 2, where the scatter increases with tunnel speed and has a range of around 2 percent at high speeds.

The measured damping estimates presented in this paper are an attempt to more effectively average out the experimental uncertainty produced by turbulence. The Prony algorithm is quite effective at extracting frequency and damping from very short segments of a free decay. Over a short enough time segment, the turbulence can be considered as a random impulse on the system. Thus, by using one-cycle segments of time history and incrementing the segment along the time history with 95-percent overlap, several hundred Prony estimates can be obtained from each free-decay measurement. The one-cycle Prony estimates from multiple free decays are then collectively pooled for a given test condition. Averages obtained from this larger pool of one-cycle Prony estimates have resulted in a more consistent estimate for the system damping than simply averaging the small number of moving-block results.

In addition, the one-cycle Prony estimates can also be sorted according to the magnitude of the wing bending moment, and then averaged to give frequency and damping as a function of vibration amplitude. An example of this is presented in Figure 2, which presents the averaged multiple-Prony estimates at wing bending moment levels of 2000, 3000 and 4000 in-lbs (±250 in-lb) in addition to the individual moving-block estimates. The damping and frequency were found to often vary significantly with vibration amplitude, likely due to the friction in the conversion bearing and hub gimbal. In this work, the curve fits presented for the damping values are based on the 3000-in-lb wing moment levels, since this level had the most available data that was above the steady-state

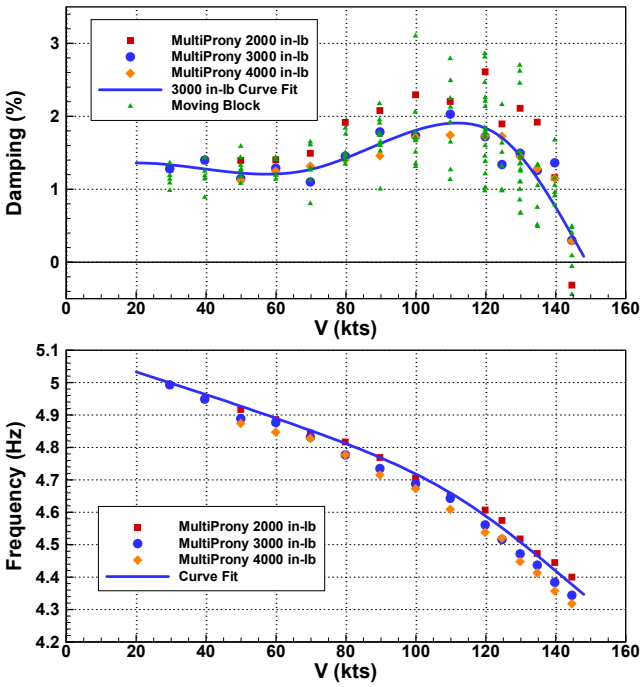

Figure 2. Example of the measured vertical-mode response as computed using various analysis methods.

turbulence vibration. The variation in frequency as a function of amplitude was found to be relatively constant. The wing-vertical frequency decreased by approximately 0.022 Hz per 1000-in-lb of wing moment, and the wing-inplane frequency decreased by 0.030 Hz for the fiberglass blades and 0.023 Hz for the carbon-fiber blades. Thus, the curve fits presented for the frequency are based on all amplitude levels having been shifted to the 2000-in-lb wing moment level.

PARAMETRIC STUDIES

The primary objective for this wind-tunnel test was quantification of the effect that pitch-flap coupling has on the stability of tiltrotors. The baseline TRAST configuration with fiberglass rotor blades was tested with δ_3 values ranging from -0° to -30°. Past studies have shown that making the pitch-flap coupling more negative typically decreases the whirl-flutter stability (Ref. 7), and this can be seen in the measured damping of the wing-vertical mode presented in Figure 3. The lines in this figure present the measured frequency and damping trends of the wing-vertical mode for the TRAST operating at 727 and 909 RPM and configured with the 4k pitch spring and the fiberglass rotor blades. As tunnel speed increases, the aeromechanical response of the rotor causes the modal frequency to decrease in a manner that is relatively independent of δ_3. For δ_3 values near zero the frequency trends begin to diverge at high airspeeds, but this occurs at a point when the modal damping has become very large.

The damping response for these fiberglass-blade configurations is typical of proprotor whirl flutter, with a large increase in damping occurring as the regressive-lag blade mode begins to interact with the wing-vertical mode (Ref. 6). As airspeed increases, the rotor collective must be increased to maintain the windmilling condition at the required rotor speed. This increase in collective in turn causes the frequency of the lag mode of the rotor blades to decrease, because the lagwise bending motion includes greater amounts of blade bending in the more compliant direction normal to the blade chord. Thus, as tunnel speed increases the regressive-lag frequency, which is the fixed-frame frequency of the asymmetric blade-lag mode, crosses the wing-mode frequency and induces an aeromechanical interaction that is very effective at removing energy from the system. For 727 RPM this can be seen in the significant increase in modal damping that occurs above 100 kts. This behavior contrasts with more classical whirl flutter in which the damping decreases monotonically with increasing airspeed. The data in Figure 3 demonstrate that less negative δ_3 not only increases stability as it would for a rigid rotor, but also changes how the regressive-lag mode interacts with the wing-vertical mode to further increase damping.

When operating at a rotor speed of 909 RPM, as opposed to 727 RPM, there are two changes to the response of the wing-vertical mode. First, the higher rotor speed causes a greater decrease in damping with increasing airspeed, because the faster blade speed induces a larger aeromechanical response. Second, the higher rotor speed requires a lower collective,

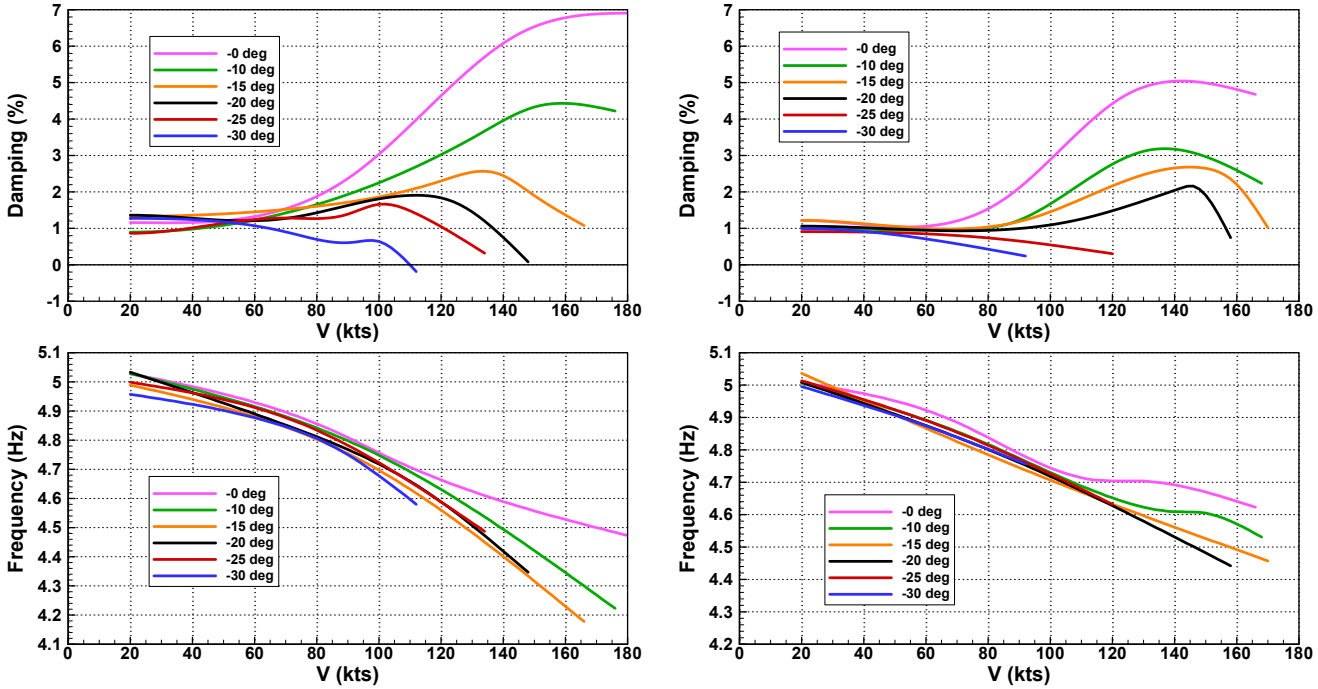

(a) 727 RPM

(b) 909 RPM

Figure 3. Measured vertical-mode response for various values of pitch-flap coupling (fiberglass blades).

thus the interaction of the regressive-lag mode with the wing-vertical mode occurs at higher airspeed. The combination of these two changes creates a counter-intuitive case at -20° δ_3 in which the lower-speed rotor goes unstable at a lower airspeed.

Comparable results for the wing-inplane mode are presented in Figure 4. This mode has significantly larger damping due to the fact that the modal motion is changing the inflow of the rotor. Also, since the frequency of this mode is higher than the wing-vertical mode, the changing regressive-lag mode interacts with it at a much lower tunnel speed (around 80 kts). While the larger damping associated with this mode typically means it does not represent a stability concern, at pitch-flap coupling values of -0° and -10° this mode has a lower stability boundary than the wing-vertical mode (compare Figures 3 and 4).

The carbon-fiber blade set was tested in combination with the 4k pitch spring and δ_3 values of -0°, -15° and -30°. The measured frequency and damping for the wing-vertical and wing-inplane modes are presented in Figures 5 and 6, respectively. Because the carbon-fiber blades are significantly stiffer than the fiberglass blades, the regressive-lag mode frequencies are much higher, and the changing collective never causes them to decrease to the point where they can interact with the wing-vertical mode. Thus, the blades can be treated as rigid, and the monotonic damping change with airspeed is governed by only the pitch-flap coupling. A more thorough discussion of the difference between the fiberglass and carbon-fiber blade sets is presented in Ref 6.

A small study was also performed to quantify the effect of air density on the damping of the wing-vertical mode. This study was conducted at a rotor speed of 909 RPM for the configuration with the 4k pitch spring, carbon-fiber blades and a pitch-flap coupling of -30°. This configuration was selected because its relatively low stability boundary minimized the scatter induced by the tunnel turbulence. Velocity sweeps were performed at tunnel pressures of approximately 1700, 1900 and 2100 psf, which corresponded to air densities of 0.00188, 0.00209 and 0.00232 slug/ft^3, respectively. Figure 7 presents both the estimated frequency and damping results for individual data points (symbols) and the curve fits estimating the frequency and damping trends for each tunnel pressure. As one would expect, decreasing the tunnel pressure, and thereby the air density, reduced the aerodynamic forces, resulting in an increase of the flutter boundary from approximately 78 kts to 100 kts as the tunnel pressure was reduced from atmospheric to 1700 psf.

Stability measurements were also performed with the 3k and 5k pitch springs for the configuration with fiberglass blades and a pitch-flap coupling of -20°. Unfortunately, it was discovered after the test that the aluminum stiffeners bonded to the composite wing spar appear to have debonded at the wing root during the middle of the 3k-pitch-spring test. This debonding resulted in a decrease in the wing stiffness, making a direct comparison between the 3k, 4k and 5k pitch springs inappropriate and are therefore not included in this

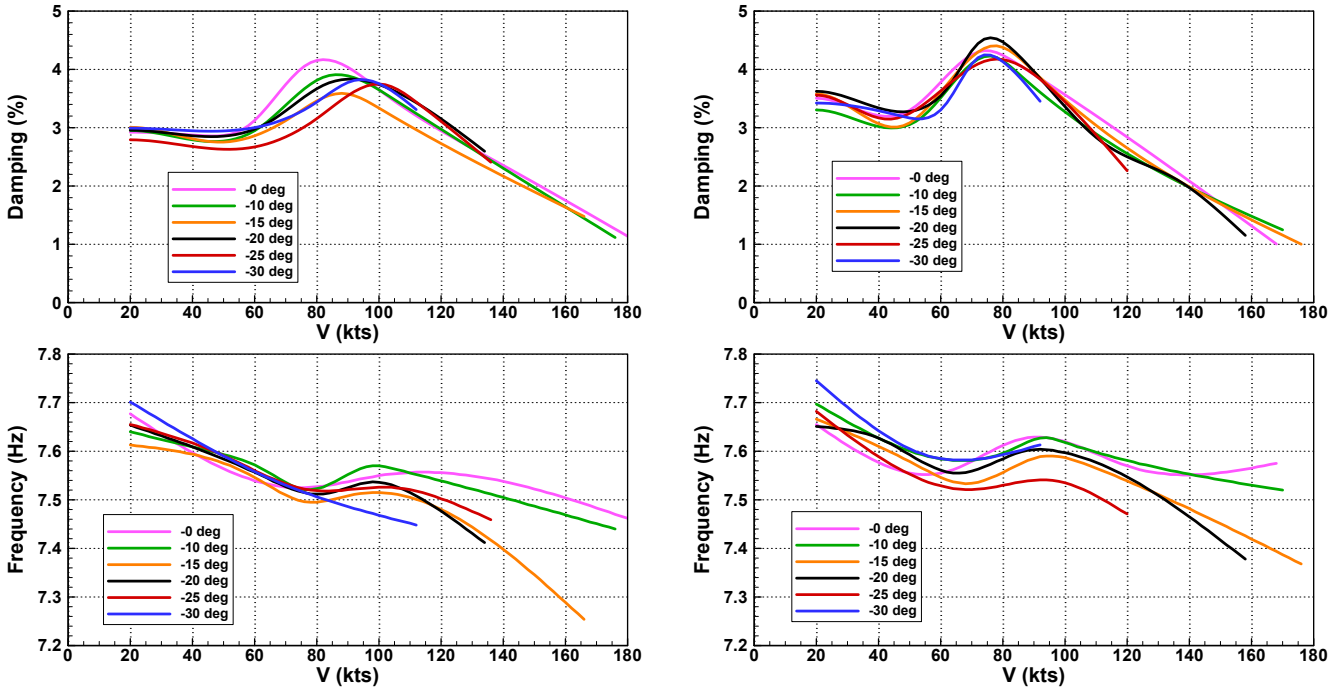

(a) 727 RPM (b) 909 RPM

Figure 4. Measured inplane-mode response for various values of pitch-flap coupling (fiberglass blades).

work. Analysis of the test results suggests that the debonding event was confined to the 3k-pitch-spring test, and so while the wing stiffness is lower, it was constant for the two 5k-pitch-spring tests that followed.

The final whirl-flutter comparison was between the two yaw-spring stiffnesses conducted using the configuration with the 5k pitch spring, fiberglass blades and a pitch-flap coupling of -20°. The damping and frequencies of the two modes are

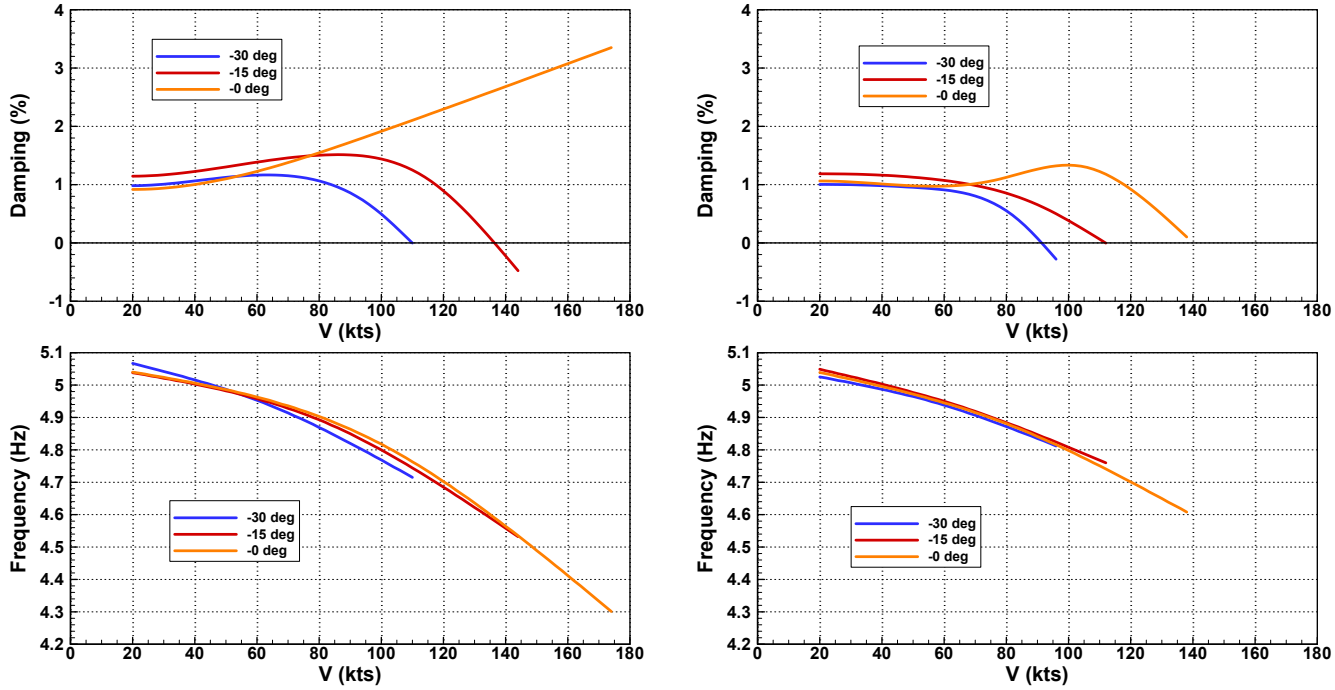

(a) 727 RPM (b) 909 RPM

Figure 5. Measured vertical-mode response for various values of pitch-flap coupling (carbon-fiber blades).

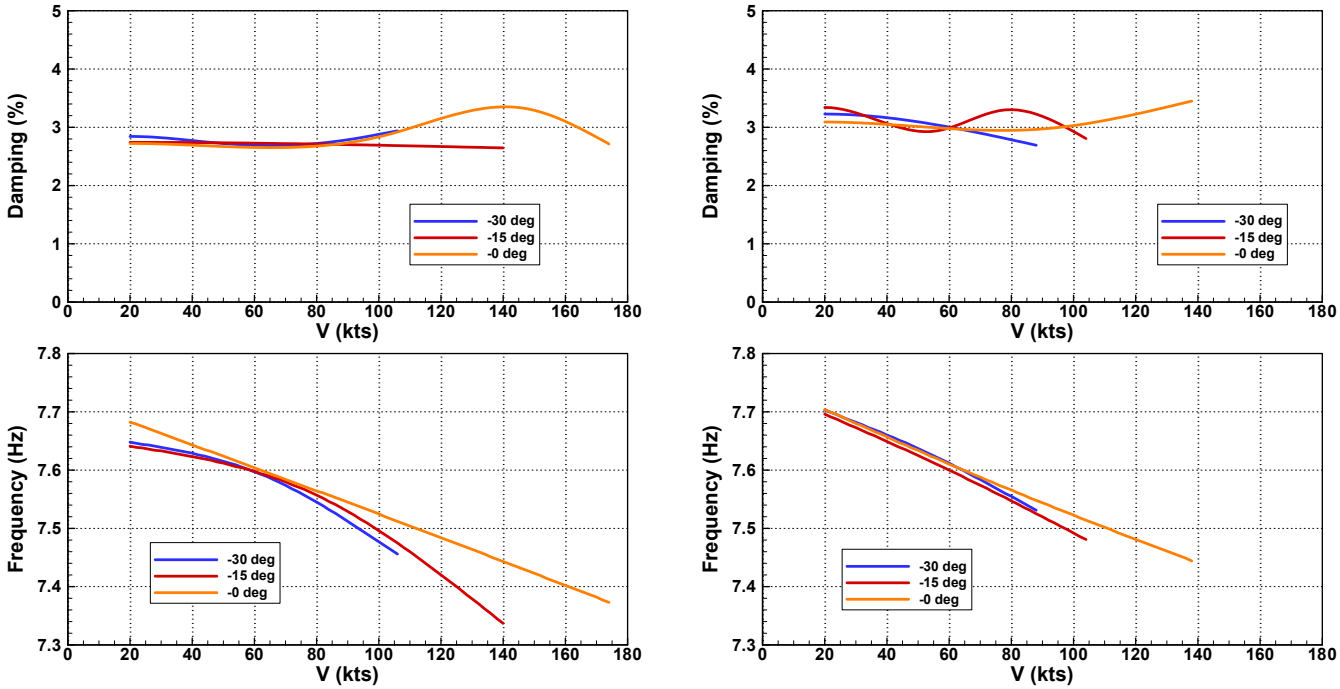

(a) 727 RPM (b) 909 RPM

Figure 6. Measured inplane-mode response for various values of pitch-flap coupling (carbon-fiber blades).

presented in Figures 8 and 9 for 727 and 909 RPM, respectively. While the reduced wing stiffness would make it challenging to use this comparison for analysis validation, the change in yaw stiffness produced a noteworthy change in response. The reduction in yaw stiffness resulted in an expected decrease in the yaw-mode frequency, but also a 0.35-Hz reduction in the wing-inplane frequency and a 0.1-Hz increase in the wing-vertical mode. The frequency changes in turn affected the wing mode interaction with the regressive-lag mode with increasing tunnel speed, and this interaction unexpectedly resulted in higher damping of both modes for the configuration with lower yaw stiffness. This observation is another example where reducing system stiffness can sometimes lead to increases in system damping, as was also seen with the fiberglass blades versus the carbon-fiber blades.

OPERATIONAL MODE SHAPES

In addition to the damping and frequency measurements, mode-shape information was also extracted from the free-decay measurements. The gimbal was instrumented with rotation sensors to provide measurement of the rotor disk motion relative to the pylon. Likewise, the pylon was instrumented with eight accelerometers that were combined using a least-squares approach to provide estimates of the rigid-body pylon motion in all six degrees-of-freedom. The coordinate origin used for the pylon motion was the point of intersection of the shaft axis and the conversion axis. The

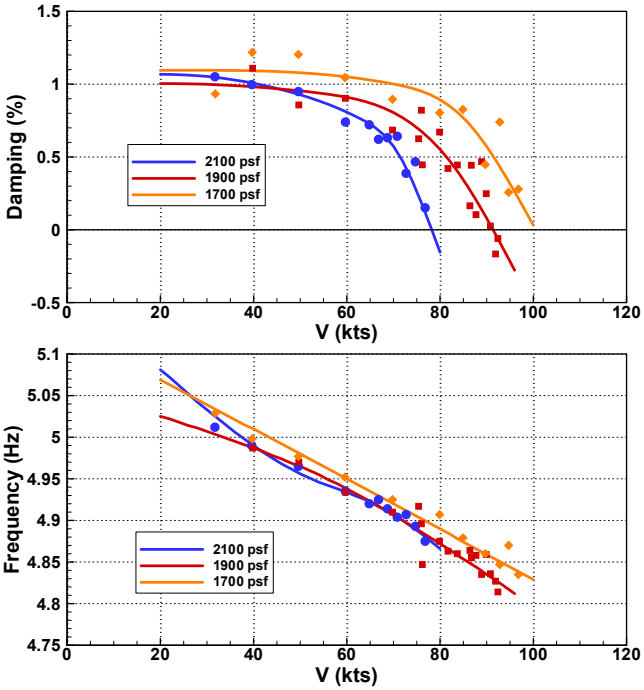

Figure 7. Measured vertical-mode response with decreasing tunnel pressure (carbon-fiber blades, -30° δ_3, 909 RPM)

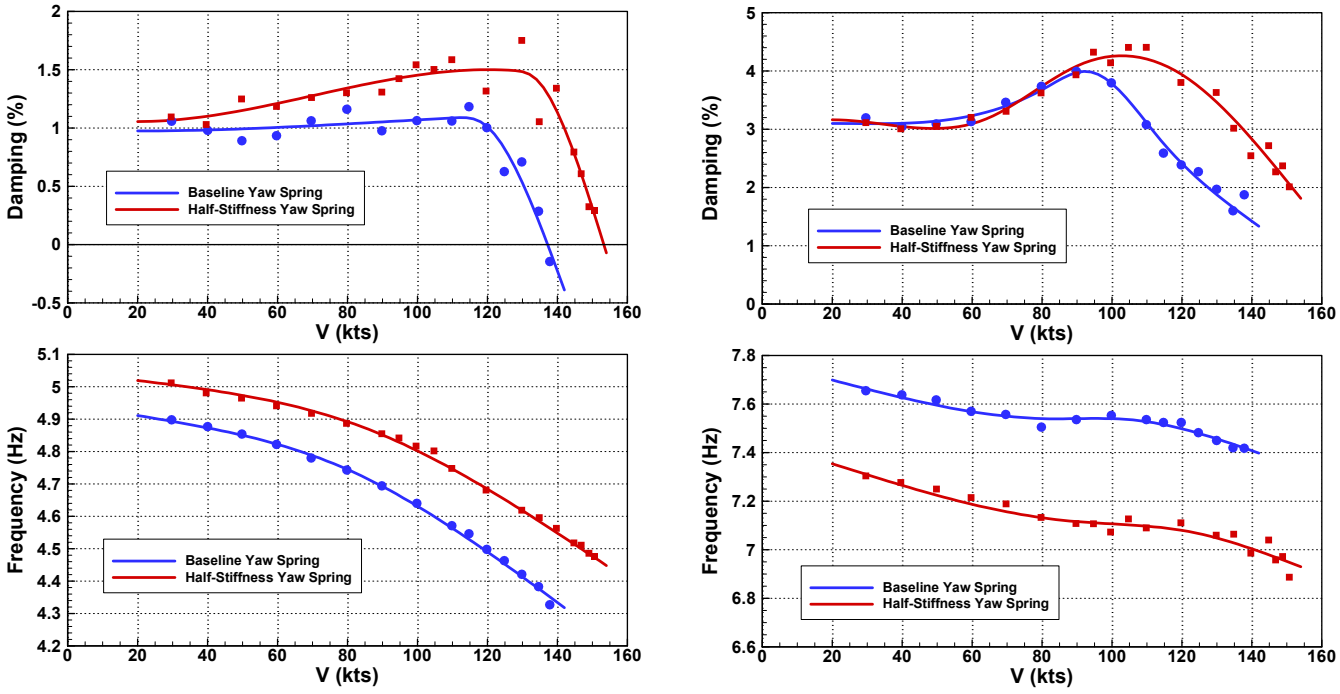

(a) Vertical Mode **(b) Inplane Mode**

Figure 8. Effect of yaw stiffness on the measured vertical and inplane modal frequencies and damping (fiberglass blades, -20° δ_3, 727 RPM).

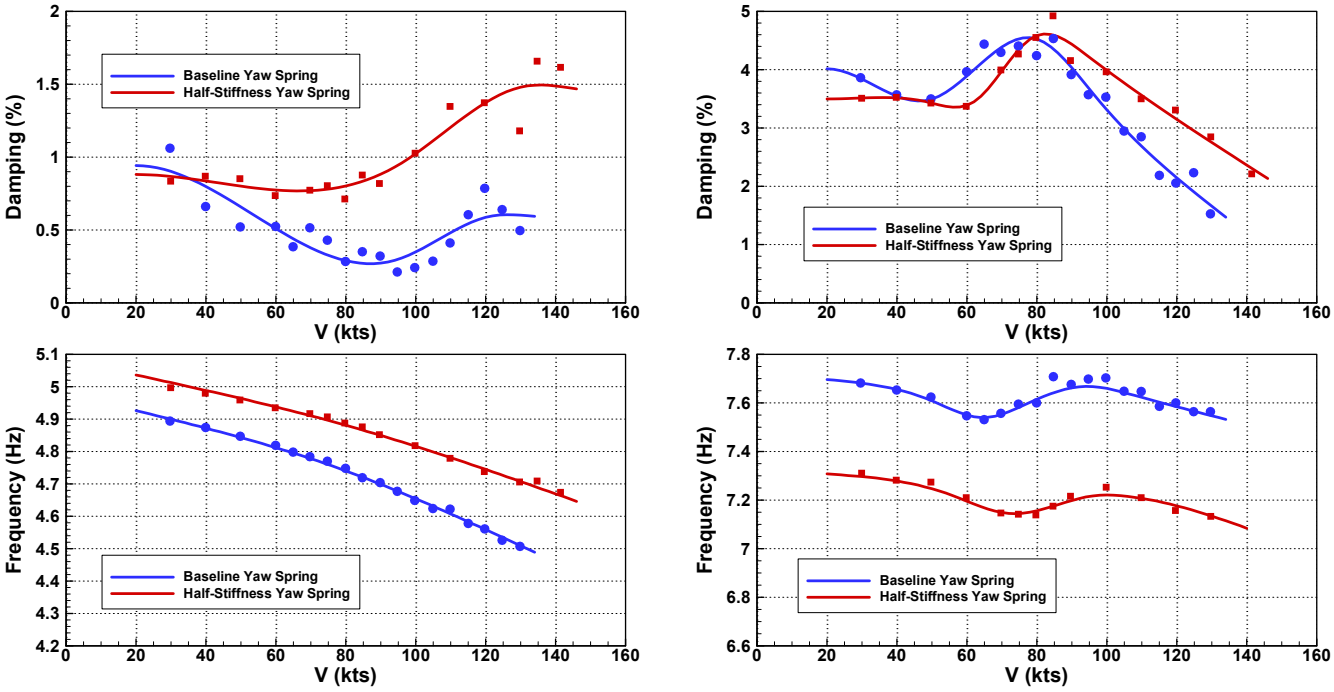

(a) Vertical Mode (b) Inplane Mode

Figure 9. Effect of yaw stiffness on the measured vertical and inplane modal frequencies and damping (fiberglass blades, -20° δ_3, 909 RPM).

accuracy of this approach was validated by comparing a set of operational pylon-motion measurements to those from a digital image correlation system.

For the wing-vertical mode, the pylon motion was found to have a relatively constant value of 0.072 in. per 1000-in-lb of wing-vertical bending moment. This value was observed to be independent of blade type, rotor speed and δ_3. However, the relative amount of pylon pitch that was measured increased with tunnel speed. Figure 10 presents the pylon pitch over the range of δ_3 angles for the configuration with fiberglass rotor blades and a rotor speed of 909 RPM. The magnitude of the pylon pitch is per 1000-in-lb of wing-vertical bending moment, and the phase angle is also relative to the wing-vertical bending moment. Given the scatter in the measured rotations, it is difficult to determine if there is any dependency on δ_3, but at higher tunnel speeds the wing-vertical mode clearly includes a greater amount of pylon pitch. In addition, the phase angle between the pylon pitch and the wing moment increases with tunnel speed. Similar trends were observed for 727 RPM and for the configurations with carbon-fiber blades (not presented).

The gimbal motion of the wing-vertical mode for the configuration with fiberglass rotor blades and a rotor speed of 909 RPM is presented in Figures 11 and 12. Although the pylon motion is predominately in the pitch direction, gyroscopic forces result in the rotor exhibiting both lateral and longitudinal disk rotation. The gimbal measurements exhibited less scatter than the pylon motion measurements, thus it is possible to discern that more negative δ_3 produces slightly less longitudinal rotation of the rotor disk and slightly more lateral motion. The longitudinal rotation is also very sensitive to friction in the gimbal. Late during the wind-

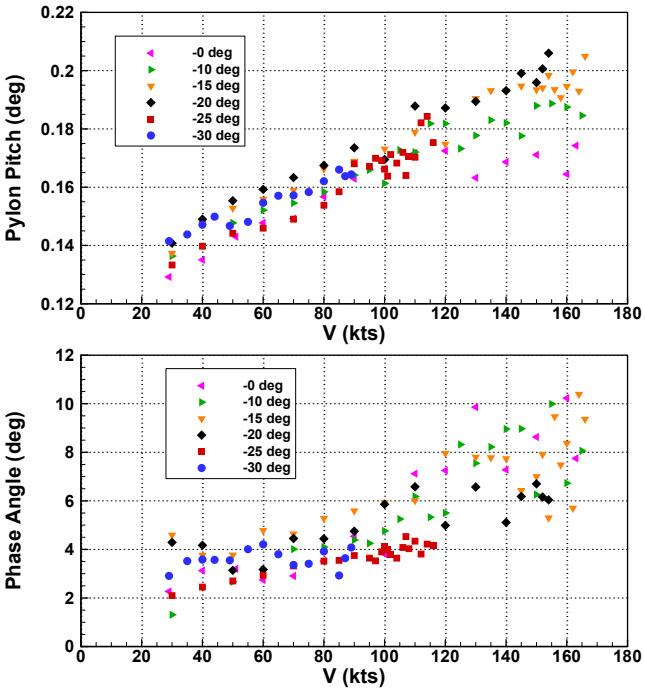

Figure 10. Measured pylon pitch per 1000-in-lb of wing moment for the fiberglass blades at 909 RPM.

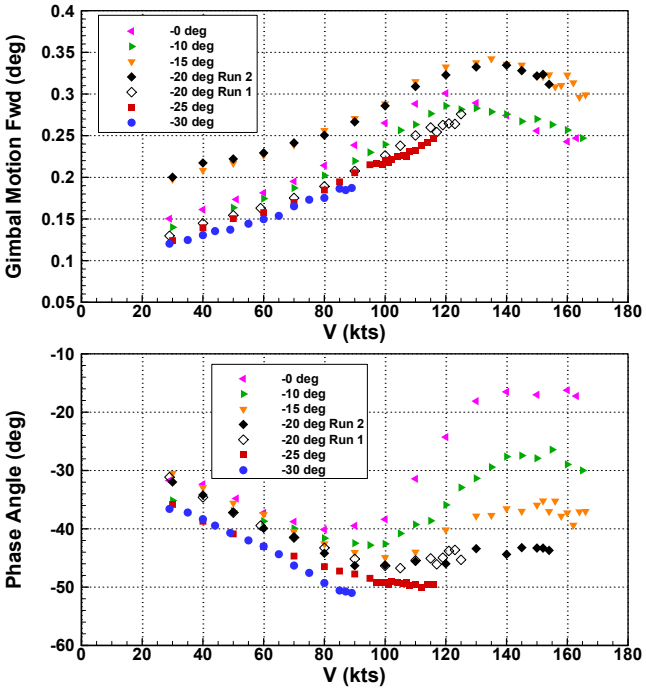

Figure 11. Measured rotor fwd/aft motion per 1000-in-lb of wing moment for the fiberglass blades at 909 RPM.

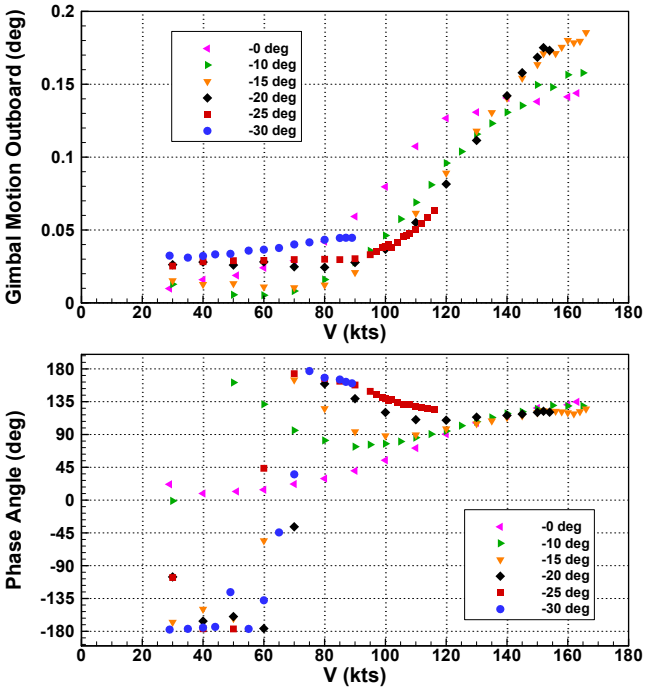

Figure 12. Measured lateral rotor motion per 1000-in-lb of wing moment for the fiberglass blades at 909 RPM.

tunnel test, the gimbal was relubricated to improve the rotor freedom of motion. Following this model maintenance, the configuration with -20° δ_3 was repeated and -15° δ_3 was tested. As a result, these two configurations had an increase of longitudinal disk rotation of about 0.06°. The kink in the magnitude of the longitudinal rotation around 130 kts appears to coincide with the crossing the regressive-lag and wing-vertical modes. Interestingly, the phase angle of the longitudinal disk rotation for the various values of δ_3 appears to exhibit very similar trends as the modal damping in Figure 3b.

OTHER MEASUREMENTS

Although the primary objective of this test was determination of experimental stability curves for validation of comprehensive modeling techniques, a large amount of other data was obtained to support this effort. Accurate whirl-flutter prediction depends on having an analytical model that captures both the structural and aerodynamic characteristics of the system, and this section presents results from some system measurements that can be used to help validate the individual components of comprehensive models. Additional component-level measurements of the TRAST can be found in Ref. 8.

As discussed above, rotor collective plays a significant role in creating the system damping with increasing airspeed. Figure 13 presents the measured collective at 727 and 909 RPM as a function of airspeed for both the fiberglass and carbon-fiber blade sets. Collective was independent of the pitch-flap coupling, and these curves are the synthesis of all the test points used in the δ_3 sweeps. There is a small difference in collective between the fiberglass and carbon-fiber blades, likely due to a small difference in the built-in blade twist produced by the fabrication process.

Because of the significance of collective, a component-level vibration test was also performed on the rotor system separate from the TRAST. The hub was suspended with the blades installed to simulate the rotor in a free-free condition (Refs. 5 and 8), and a temporary fixture was used to set the pitch of each blade. In this manner, the modal frequencies were measured across the full collective range of the rotor and are presented in Figure 14.

In addition, during the test an attempt was made to measure the highly damped regressive-lag frequency as a function of airspeed for several configurations. The rotor lag response was not clearly visible in the free-decay measurements, but resonance peaks were observed in the blade-bending moments when steady sinusoidal oscillations were applied to the swashplate. So, frequency response functions (FRFs) were produced by measuring the lagwise blade moment while stepping through a range of actuation frequencies in the vicinity of the anticipated regressive-lag frequency. Examples of the resulting FRFs across multiple airspeeds are presented in Figure 15 for the configuration operating at 909 RPM with the 4k pitch spring, fiberglass blades and a pitch-flap coupling of -10°. As airspeed and collective increase, the resonant peak in the blade-bending moment shifts downward in frequency and interacts with other system modes.

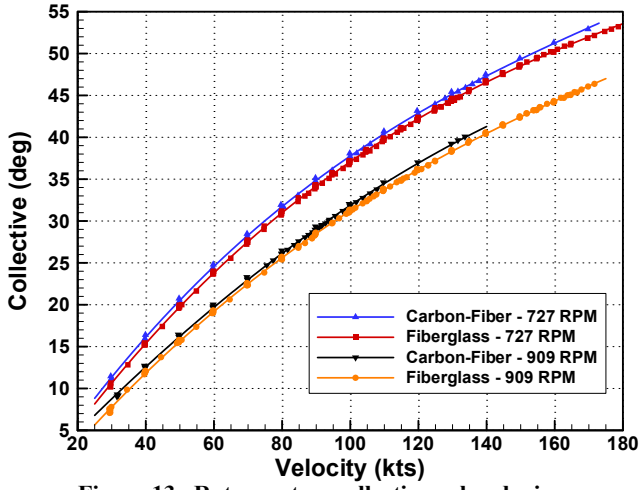

Figure 13. Rotor system collective value during windmilling operation.

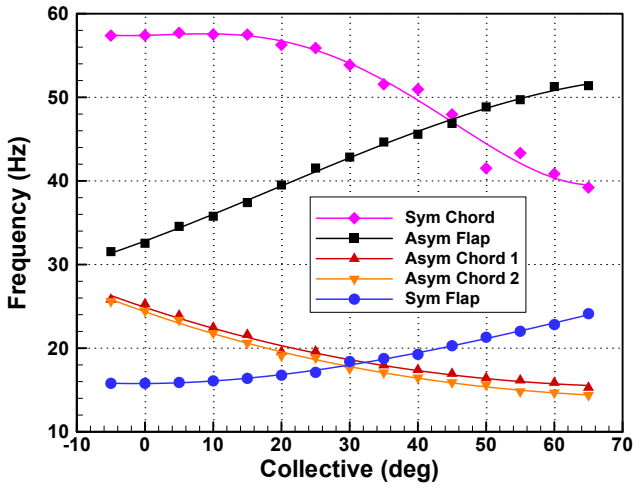

Figure 14. Measured fiberglass blade frequencies for the free-free hub and rotor system.

By using a modal curve fitter on each FRF, the regressive-lag frequency was computed for each test condition. A collection of measured frequencies as functions of tunnel speed is presented in Figure 16. In addition to the 909 RPM case discussed above, results are presented for 727 RPM, but with a pitch-flap coupling of -20°, and for 818 RPM with the half-yaw configuration whose data was previously presented in Figure 8. The multiple differences in the configurations make comparisons of these results difficult, but the novelty and time-consuming nature of these measurements meant that they were acquired during gaps in the broader test plan. The jump in measured frequency from above 10 Hz to below 9 Hz occurs when the lag frequency crosses the pylon-pitch/wing-torsion mode. A similar jump can be seen in the results for 909 RPM at approximately 75 kts where the lag frequency crosses the wing-inplane mode. This data is not typically measured for tiltrotors, but it should be very valuable in the validation of compressive modeling tools.

System damping is determined by not only rotor aeromechanics, but also by the aeroelastic response of the wing and pylon. To quantify the magnitude of this response and identify how it changes with airspeed, stability measurements were also performed on the TRAST without rotor blades installed. The wing-vertical mode was excited by using oscillations of the aileron built into the wing, and the wing-inplane mode was excited by using the inertial mass of the swashplate. The stability of the wing-inplane mode was unaffected by airspeed and had a constant frequency and damping of 8.01 Hz and 0.90 percent. The frequency and damping of the wing-vertical mode are presented in Figure 17. Interestingly, tunnel turbulence had a greater effect on the model without the rotor installed, and this resulted in a large amount of scatter in the damping measurements. Despite this, there does seem to be a trend in which the wing aerodynamics causes modal damping to increase with increasing airspeed from 0.5 percent to approximately 0.9 percent at 110 kts. Thus, it may be necessary to include wing aerodynamics in comprehensive models to accurately predict the whirl-flutter boundary.

To verify the structural dynamics of the TRAST without aerodynamic effects, at least one set of rap tests was performed on the model for every configuration tested. To ensure that the results corresponded to the operational characteristics of the model, the tests were conducted with

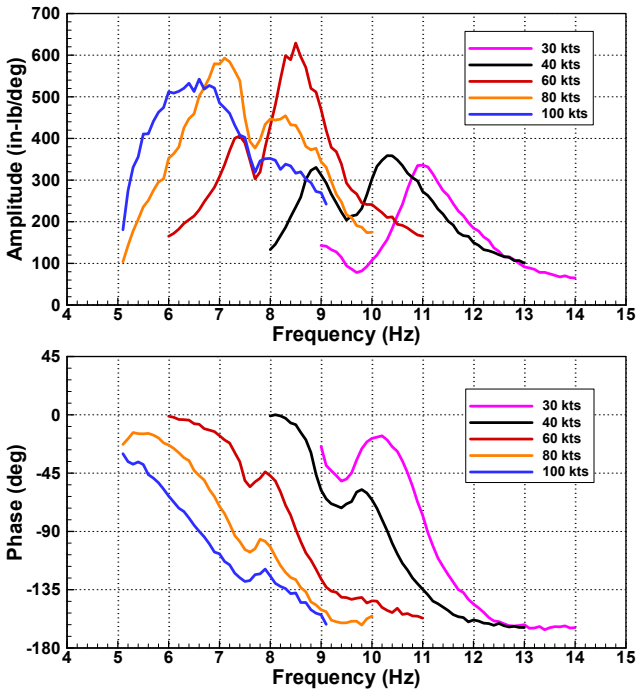

Figure 15. Measured blade-bending moment FRFs for sinusoidal swashplate oscillation (fiberglass blades, -10° δ_3, 909 RPM).

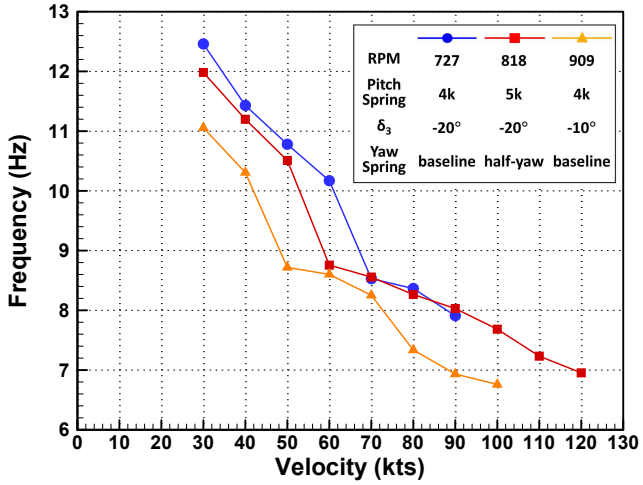

Figure 16. Measured regressive lag frequency for various fiberglass-blade configurations and rotor speeds.

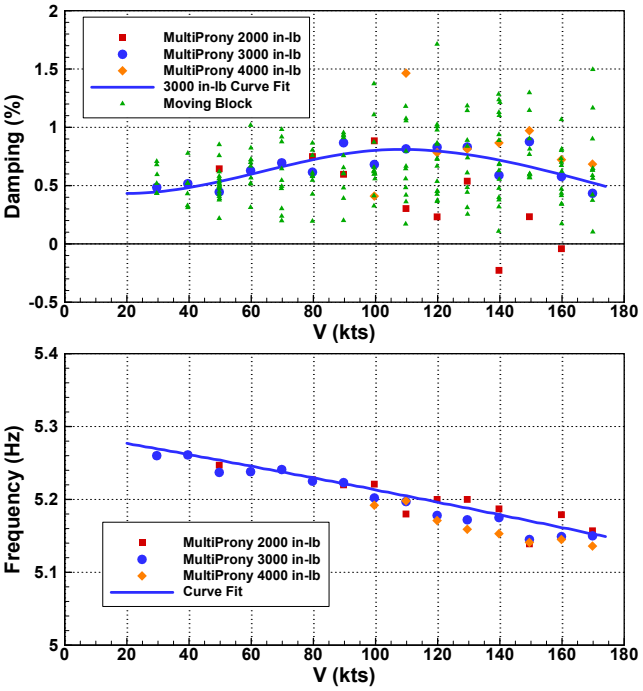

Figure 17. Measured vertical-mode response without rotor blades (5k pitch spring).

the blades installed immediately following wind-tunnel runs where the model had sufficient time to warm up. These rap tests involved shaking or hitting the model to excite the primary modes and extracting the frequency and damping from the measured free decay. While the pitch spring and yaw spring obviously affected the structural response, the frequency and damping were observed to be independent of the pitch-flap coupling. Results for the 4k pitch spring are summarized in Table 2, which includes the measurements for all values of δ_3 that were tested. It should be noted that even though the rotor is gimballed and has a very soft gimbal spring, the flexibility of the fiberglass blades did result in the system having slightly lower frequencies than when the carbon-fiber blades were installed.

Table 2. Nonoperational modal parameters measured in the TDT with the 4k pitch spring.

	Fiberglass Blades			
	Frequency (Hz)		Damping (%)	
	Mean	Std Dev	Mean	Std Dev
Wing Vertical	4.97	0.03	1.29	0.15
Wing Inplane	7.58	0.02	1.61	0.23
Pylon Pitch	8.93	0.18	3.80	0.49
Pylon Yaw	16.50	0.16	1.74	0.19
	Carbon-Fiber Blades			
	Frequency (Hz)		Damping (%)	
	Mean	Std Dev	Mean	Std Dev
Wing Vertical	5.01	0.01	1.21	0.02
Wing Inplane	7.62	0.02	1.59	0.09
Pylon Pitch	9.21	0.03	3.68	0.15
Pylon Yaw	16.61	0.12	1.93	0.26

CONCLUSIONS

The second wind tunnel test of the TiltRotor Aeroelastic Stability Testbed (TRAST) was conducted at the Langley Transonic Dynamic Tunnel from October to December 2023. The primary objective of this test was to conduct a parametric study of pitch-flap coupling and to quantify its effect on the stability of tiltrotors. Secondary test objectives included parametric studies of rotor blade stiffness, test medium density, pitch spring stiffness and wing-pylon joint yaw stiffness. These studies will be utilized to guide and validate comprehensive model development of future tiltrotor aircraft.

Major findings of the parametric studies included:

1. Varying the pitch-flap coupling angle (δ_3) from -0° to -30° demonstrated how the regressive-lag mode can couple with the wing modes to significantly increase system damping, and how pitch-flap coupling affects this interaction.
2. The higher compliance of fiberglass blades compared to carbon-fiber blades increased system damping. The stiffer carbon-fiber blades raised the regressive-lag mode frequency and thereby limiting its interaction with the wing modes.
3. Reducing the test medium density increased the stability boundary, with minor impact on frequency.
4. Reduction in wing-pylon yaw stiffness changed the interaction of the regressive-lag mode and wing-vertical mode, resulting in an increase in damping of both modes.

In addition to the parametric studies, a variety of supporting measurements were performed to aid the validation of comprehensive models. These included velocity-dependent frequency and damping trends of the wing and pylon without

rotor blades, the regressive-lag mode characterization at multiple airspeeds, and isolated-rotor frequencies determined through a free-free rotor system ground vibration test.

REFERENCES

1. Kreshock, A. R., Thornburgh, R. P., Wilbur, M. L., Kang, H., Piatak, D. J., and Sekula, M. K., "Initial Whirl-Flutter Characterization of the TiltRotor Aeroelastic Stability Testbed," Proceedings of the VFS 79th Annual Forum, West Palm Beach, FL May 16-18, 2023.
2. Akinwale, A., Datta, A., "High Speed Whirl Flutter Tests of the Maryland Tiltrotor Rig," Proceedings of the VFS 79th Annual Forum, West Palm Beach, FL, May 16-18, 2023.
3. O'Brien, N., Datta, A., "Aeroelastic Stability of a Hingeless Hub Tiltrotor at High Speeds," Proceedings of the VFS 80th Annual Forum, Montreal, Quebec, Canada, May 7-9, 2024.
4. Hoff, S., Fonte, F., Soal, K., Schneider, O., Kapteijn, K., "Whirl Flutter Testing of ATTILA Tiltrotor Testbed – Initial Results," Proceedings of the VFS 80th Annual Forum, Montreal, Quebec, Canada, May 7-9, 2024.
5. Thornburgh, R. P., and Kreshock, A. R., "Structural Modeling and Validation of the TiltRotor Aeroelastic Stability Testbed," Proceedings of the AIAA Science and Technology Forum and Exposition (AIAA SciTech 2024), Orlando, FL, January 8-12, 2024.
6. Kreshock, A. R., Thornburgh, R. P., Kang, H., and Yeo, H., "Experimental and Analytical Comparison of Stiff and Flexible Rotor Blades for Tiltrotor Whirl-Flutter Stability," Proceedings of the 50th European Rotorcraft Forum, Marseille, France, September 10-12, 2024.
7. Kvaternik, R. G., "An Experimental and Analytical Investigation of Proprotor Whirl-Flutter," NASA Technical Paper 1047, December 1977.
8. Kreshock, A. R. and Thornburgh, R. P., "Ground Vibration Testing of the TiltRotor Aeroelastic Stability Testbed," NASA Technical Memorandum-20240004747, Nov 2024.